An assessment of the effect of sea surface surfactant on global atmosphere-ocean CO_2 flux

Wu-ting Tsai[1]
Institute of Hydrological Sciences, National Central University, Jungli City, Taoyuan, Taiwan

Kon-Kee Liu[2]
Institute of Oceanography, National Taiwan University, Taipei, Taiwan

Received 30 November 2000; revised 16 November 2001; accepted 12 July 2002; published 26 April 2003.

[1] We assess the possible impact of the distribution of naturally occurring surfactants on the direct integration of the global atmosphere-ocean CO_2 flux across the ocean surface. The global atmosphere-ocean CO_2 flux is calculated using the monthly mean ΔpCO_2 climatology compiled by *Takahashi et al.* [1997] as well as satellite wind speed and sea-surface temperature data. In the absence of any global map of surfactant coverage and as it is known that phytoplankton exudates and degradation products are the major sources of marine surfactants, ocean primary productivity, which can be derived from the satellite-based estimate of chlorophyll concentration, is used as an indicator of the presence of surfactants as proposed by *Asher* [1997]. From the calculated results it is found that suppression of the upward and downward CO_2 fluxes by marine surfactants exhibits an asymmetric effect: The average percent reduction of absorption flux by surfactants is about twice that of outgassing, which results in an overall decrease in the net global CO_2 uptake by the oceans. For almost half of the year (between January and May) the presence of surfactants does not affect CO_2 outgassing from global oceans. In contrast, throughout the entire year the presence of surfactants suppresses CO_2 absorption by the oceans. The major reduction in absorption fluxes occurs in the northern Pacific and Atlantic (10°N to 70°N) in all seasons and in the Southern Ocean (south of 40°S) in austral spring and summer. However, the most significant decrease in outgassing fluxes occurs in the equatorial and southern Pacific Ocean (40°S to 10°N), particularly in the eastern equatorial and subtropical waters off the southern American coast, in the period of austral spring and summer. Annual net CO_2 flux is reduced by approximately 20% under the surfactant coverage condition that the primary productivity is above a threshold value of 25 g-C m^{-2} mom^{-1} and by about 50% with a threshold of 15 g-C m^{-2} mom^{-1}. *INDEX TERMS:* 0312 Atmospheric Composition and Structure: Air/sea constituent fluxes (3339, 4504); 4504 Oceanography: Physical: Air/sea interactions (0312); 4806 Oceanography: Biological and Chemical: Carbon cycling; *KEYWORDS:* gas exchange, surfactant, carbon dioxide, air-sea interaction

Citation: Tsai, W.-T., and K.-K. Liu, An assessment of the effect of sea surface surfactant on global atmosphere-ocean CO_2 flux, *J. Geophys. Res.*, *108*(C4), 3127, doi:10.1029/2000JC000740, 2003.

1. Introduction

[2] The quantitative estimation of CO_2 flux across the global oceans has long been the subject of heightened interest and vigorous research (e.g., *Tans et al.* [1990] and *Takahashi et al.* [1997], among many others). The most direct way to calculate the net CO_2 flux from the ocean to the atmosphere is to integrate the local transfer rate $F = k \times s \times \Delta pCO_2$ over the global ice-free ocean surface, where k is the transfer velocity of CO_2 across the water-air interface, s is the solubility of CO_2 in bulk water, and $\Delta pCO_2 = pCO_{2w} - pCO_{2a}$ represents the gradient of CO_2 partial pressure across the interface. Uncertainties in the calculations, however, involve errors in the interpolation of ΔpCO_2 maps from the limited number of measurements and the variables involved in parameterizing the functional representation of the flux. Efforts to fill the discontinuities in the data and to construct ΔpCO_2 maps have previously been made using different techniques, such as the numerical interpolation scheme based on the advection fields of *Takahashi et al.* [1995] and the objective mapping technique of *Lefèvre* [1997]. With regard to the functional representation of flux, adjustments to improve the formulation and therefore account for realistic processes include the thermal skin effect [e.g., *Robertson and Watson*, 1992; *Van Scoy et al.*, 1995] and chemical enhancement [e.g., *Boutin et*

[1]Also at Department of Civil Engineering, National Chiao Tung University, Hsinchu, Taiwan.
[2]Also at National Center for Ocean Research, Taipei, Taiwan.

0148-0227/03/2000JC000740

al., 1999]. In this study, retardation of gas transfer by naturally occurring surfactants (surface-active matters), which are ubiquitous in the global oceans, is considered in the formulation, and the resulting impact of the distribution of surfactants on the direct integration of global CO_2 flux is assessed.

[3] The accumulation of surfactants at the water surface induces surface-tension gradients, which then modify both momentum and mass transports in close proximity to the water surface. There is considerable experimental evidence to show that the presence of surfactants drastically reduces the rate of gas transport across the water surface [e.g., *Asher and Pankow*, 1986; *Goldman et al.*, 1988; *Frew et al.*, 1990]. It is now recognized that such an impact of surfactants in retarding gas exchange is hydrodynamic in nature [*Frew et al.*, 1990] and does not involve the formation of a monomolecular barrier at the interface impeding the gas diffusion. Such a hydrodynamic mechanism is caused by the physicochemical interaction between the surfactants and the underlying turbulent flows [*Davies*, 1966]. Recent numerical validations [*Tsai*, 1996, 1998] confirm this explanation and show that an induced boundary layer, which is attributed to the inhomogeneity of surfactant distribution induced by impinging eddies, blocks the intermediate surface renewal processes of the eddies.

[4] Despite the obvious effect of marine surfactants on retarding air-sea gas exchange, attempts to incorporate such a process in the calculation of global oceanic CO_2 uptake are much less than those efforts associated with the effects of thermal skin and chemical enhancement. The calculation of *Asher* [1997] has, in fact, been the only effort so far. The major obstacles in quantitatively estimating the surfactant effect on atmosphere-ocean CO_2 flux result from the absence of distribution maps of surfactant coverage, including the extent and concentration, over the global oceans, as well as the nonexistence of a unique parameterization of transfer velocity in the presence of marine surfactants. To assess the impact of the naturally occurring surfactants on global ocean CO_2 flux, a simplified model was proposed by *Asher* [1997] to account for the influence of surfactants. In the model the dependence of the reduction rate of gas transfer on the in situ surfactant concentration is relaxed, and the influence is determined solely by the presence of surfactants. Whether the surface is surfactant-covered or not is then assumed to be determined by the extent of biological activity based on the arguments which follow.

[5] The major source of oceanic surfactants is from marine phytoplankton, while other input, such as atmospheric and anthropogenic pollution, only contribute minimal amounts. It has been shown that various marine phytoplankton are capable of producing surface-active materials as metabolic by-products, although not all species are equally productive [*Wilson and Collier*, 1972; *Žutić et al.*, 1981]. The field observations of *Žutić et al.* [1981] found that a significant positive correlation exists between local surfactant activity and phytoplankton density. A recent experiment by *Gašparović et al.* [1998] has given further support for this by showing that the most important source of surfactants is the organic matter produced by the present plankton and bacteria and promoted by sunlight.

[6] Surfactants are known to effectively attenuate surface roughness and consequently reduce radar backscatter. Thus further evidence can be provided by cross examining satellite images respectively associated with surface roughness and biological activity variables, such as images of synthetic aperture radar and ocean color. Such a multiple-sensor comparison has recently been demonstrated by *Liu et al.* [2000] and *Lin et al.* [2002] using ERS-2 SAR and SeaWiFS images. The results reveal a close matching of the boundaries between the two images and also indicate a strong correlation between the reduction of normalized radar cross section of ERS-2 SAR and the chlorophyll-a concentration of SeaWiFS data. This correlation is supported by simultaneously acquired in situ sea truth measurements which quantify the relationship between the reduced radar backscatter and enhanced chlorophyll concentration, and it further confirms that the attenuated surface roughness is indeed attributed to surfactants produced during active phytoplankton growth.

[7] The potential relation between the biological productivity and the reduction in the air-water gas exchange was first elucidated by the laboratory measurements of *Goldman et al.* [1988] who measured the oxygen evasion rates for different natural seawaters in a small tank mixed by means of a vigorous sloshing motion. They noted that the reduction rates of transfer velocity increase from the waters of the open oceans towards the estuarine waters which have a similar pattern of variation with regard to biological productivity. In that there are no global maps illustrating the marine surfactant coverage, the distribution of phytoplankton primary productivity, which can be derived from satellite-based estimates of chlorophyll concentration, seems to be an applicable substitute to characterize the presence of surfactants, as proposed by *Asher* [1997]. In the present work, following the calculations of *Asher* [1997], an area of the ocean surface is considered covered by surfactants if the local primary productivity is higher than a chosen threshold.

[8] The data used in the study of *Asher* [1997] were yearly averaged climatological maps. The purpose of that work was to demonstrate the possible effects of surfactant coverage as well as the geographical variability of the coverage on the global air-sea CO_2 flux estimates. In addition, strong seasonal variations in the distributions of wind field and ΔpCO_2 further complicate the influence of the surfactants on the CO_2 flux calculation. As a result, it is worth it to reappraise the influence of marine surfactants on the global atmosphere-ocean CO_2 flux by considering seasonal variations in the calculations. In this study the calculations of *Asher* [1997] are refined by employing the recently published ΔpCO_2 climatology and the satellite wind, SST, and ocean color data. Both seasonal and geographical variations in the impact of surfactants on the global CO_2 exchange coefficient and flux are emphasized. In particular the variabilities and comparative magnitudes of the reduction in fluxes associated with both outgassing to the atmosphere and absorption by the oceans are discussed.

2. Integration of Global CO_2 Flux

[9] The transfer velocity, k, which is governed by both turbulent transport and molecular diffusion, is traditionally parameterized by the wind velocity at the height of 10 m, U_{10} and the Schmidt number, $Sc = \nu/D$, where ν is the kinematic viscosity of water and D is the diffusion coef-

ficient of CO_2 in water. Two widely used empirical functional representations of $k = k(U_{10}, Sc)$ are (1) the three-regime, piecewise linear relation between k and U_{10} of *Liss and Merlivat* [1986] who synthesized and extrapolated the data of the wind-tunnel experiments by *Broecker and Siems* [1984] and *Merlivat and Memery* [1983] as well as the tracer gas (SF_6) exchange experiment of *Wanninkhof et al.* [1985] and (2) the quadratic dependence of k on U_{10} of *Wanninkhof* [1992] based on the field data of the ^{14}C measurements. The difference between the quasi-linear and the quadratic relationships is on average a factor 1.6 but it is larger at low wind speeds than at moderate range. The *Liss and Merlivat* [1986] relationship (denoted by k_L) is employed in most of the calculations here as it was based on data corresponding to processes which take place on much shorter time and space scales compared with those of ^{14}C data. For comparison, the Wanninkhof's relationship (denoted by k_W) is also used in some calculations, which will then be noted in the text. The choice between these two parameterizations of U_{10} and k, however, is not critical in this study, since the primary objective here is to assess the relative impact of surfactants on global CO_2 flux calculations.

[10] Much less measured data of k-U_{10} relationship in the presence of surfactants are available than for a clean interface. *Broecker et al.* [1978] measured the transfer velocity of CO_2 in a linear wind-wave tunnel covered by a monolayer of oleyl alcohol. Adopting the experimental data of *Broecker et al.* [1978] and the finding of *Jähne et al.* [1987a] that the presence of a surfactant increases the Sc exponent to 2/3, *Asher* [1997] proposed a linear relationship:

$$k = 2.778 \times 10^{-6}(1.04U_{10} - 0.12)\left(\frac{Sc}{600}\right)^{-2/3}, \qquad (1)$$

(k in m s^{-1}) to the limit of the measurements of *Broecker et al.* [1978] at the wind speed of 12.5 m s^{-1}. In the present work, the measured data of the reduction rate of k due to the presence of surfactants, as reported by *Broecker et al.* [1978], are made use of and are extrapolated to the limit of vanishing wind velocity by fitting the data with a power curve of U_{10}. The data fitting finds that the best curve of the reduction rate r is

$$r = 0.56U_{10}^{-0.13}. \qquad (2)$$

This reduction rate of k is assumed to be applicable for regimes of smooth ($U_{10} < 3.6$ m s^{-1}) and rough (3.6 m s^{-1} $< U_{10} <$ 13 m s^{-1}) water surfaces as identified by *Liss and Merlivat* [1986].

[11] For wind speeds greater than 13 m s^{-1}, continuous surfactant films begin to tear [*Broecker et al.*, 1978], and wave breaking might also occur. If the ocean surface is free of surfactants, the air-water gas exchange rate is enhanced by bubbles generated in the process of wave breaking, and a higher k-U_{10} slope can be observed like that in the relationship of *Liss and Merlivat* [1986]. Breaking waves certainly disrupt the surfactant effect on retarding air-sea gas exchange by dispersing or tearing insoluble surface films. Even so, a marine surface microlayer could be composed of soluble surfactants which can reabsorb to the ocean surface once the surface films are disrupted by breaking waves. Moreover, soluble surfactants have been shown to be as effective as insoluble ones in inhibiting gas exchange [*Goldman et al.*, 1988; *Frew et al.*, 1990]. This implies that the transfer velocity k across a surfactant-covered ocean surface could still be decreased even in the presence of breaking waves at relatively high wind speeds. This has been supported by the experiments of *Asher et al.* [1996] which were conducted in a whitecap simulation tank. The drastic deviation of the near-surface process from non-breaking free-surface turbulence to bubble-mediated flow is also indicative of an abrupt change in the hydrodynamic mechanism of the surfactant effect. A critical wind speed is therefore anticipated in the surfactant-influenced k-U_{10} parameterization, and this should reveal changes in the transfer process as well as the surfactant effect.

[12] Although such characteristics of the surfactant effect have frequently been observed in surfactant contaminated and natural waters, few experiments have ever addressed the issue quantitatively. *Broecker et al.* [1978] reported that at wind speeds greater than 13 m s^{-1}, the surfactant film begans to tear. Broecker et al. did not report any quantitative data on the reduction rates beyond this critical wind speed, however. In order to mimic such transitional characteristics and also maintain the continuation of the surfactant effect in the parameterization for wind speeds greater than 13 m s^{-1}, here a similar k-U_{10} slope of clean surface is assumed for a surfactant-covered water surface. This yields

$$k = 2.778 \times 10^{-6}(5.9U_{10} - 70.7)\left(\frac{Sc}{600}\right)^{-1/2}, \qquad (3)$$

(k in m s^{-1}) for the surfactant-influenced parameterization of *Liss and Merlivat* [1986]. Figure 1 compares the present surfactant-influenced k-U_{10} relationship with other parameterizations. Note that the reduction rate, $r = 21.4/(5.9U_{10} - 49.3)$, decreases with increasing wind speed in equation (3).

[13] The measurement of the oxygen transfer velocity conducted in an annular wind-wave channel with seawater collected at various locations along productivity gradients indicated that no unique k-U_{10} relationship is likely to exist for natural waters containing surface-active matters (unpublished data of Frew, Goldman, and Bock given by *Frew* [1997]). The result presented by *Frew* [1997] also shows that the critical wind speed at which the surfactant-influenced water surface rapidly becomes developing waves and eventually breaks as the wind continues to increase is dependent on the concentration of surfactants. Recent measured transfer velocities for oxygen evasion in circular wind-wave flumes in the presence of synthetic surfactants [*Bock et al.*, 1999] revealed that the functional relationship of k-U_{10} may also depend on the concentrations of surfactants. Despite these uncertainties, several measurements point to reduction rate with a quantitative range: *Bock et al.* [1999] reported the highest reduction rate of 60% at a given wind friction velocity in their experiments conducted in circular flumes covered with soluble surfactants (Triton X100). Similar experiments by Frew, Goldman, and Bock (unpublished data given by *Frew* [1997]), however, showed

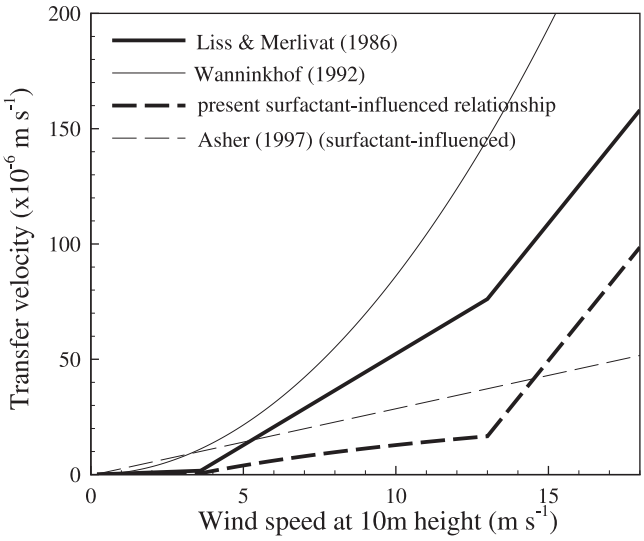

Figure 1. Gas transfer velocity k (m s^{-1}) versus wind speed U_{10} (m s^{-1}) for clean and surfactant-covered ocean surfaces. The thick and thin solid lines represent the quasi-linear parameterization of *Liss and Merlivat* [1986] and the quadratic one of *Wanninkhof* [1992], respectively. The thin dashed line is the surfactant-influenced k-U_{10} relationship (equation (1)) used in the calculation of *Asher* [1997]. The thick dashed line is the surfactant-influenced k-U_{10} relationship used in the present assessment which is derived by applying the reduction rate in equation (2) to the quasi-linear relationship of *Liss and Merlivat* [1986] for the wind speeds from 0 to 13 m s^{-1} and continuing to higher speeds, assuming a similar k-U_{10} slope of clean surface.

considerably higher reduction rates, as high as 90% at the critical wind speed. The laboratory measurements of the oxygen evasion rates [*Goldman et al.*, 1988] across an unsheared turbulent air-water interface, a somewhat different hydrodynamic process from the wind enhanced transfer, revealed reduction rates ranging from 5 $\sim$ 15% for oceanic waters to 50% for nearshore waters. Similar experiments in a stirred air-water system by *Frew et al.* [1990] for surfactants generated by various species of marine phytoplankton also observed 5 to 50% decreases in the oxygen evasion rates depending on the species.

[14] The fitted curve in equation (2), representing the relationship between the wind speed U_{10} and the reduction rates of the CO_2 transfer velocity r, is based on the measurements of *Broecker et al.* [1978] which were conducted in a large linear wind-wave tunnel with the presence of insoluble surfactants (oleyl alcohol). For the range of the most frequently occurring wind speeds over the global oceans, the reduction rate increases asymptotically from $\approx$70% at U_{10} = 5 m s^{-1} to $\approx$75% at U_{10} = 10 m s^{-1}. At the assumed critical wind speed of U_{10} = 13 m s^{-1}, the reduction rate r $\approx$80%. Due to the lack of any better measured data than those of *Broecker et al.* [1978], the reduction rate in equation (2) is used to represent an approximation of the average effect of the surfactants in our assessment with the understanding of the complexity in surfactant-influenced k-U_{10} parameterization.

[15] In the calculation of the CO_2 flux, $F = k(U_{10}, Sc) \times s \times \Delta pCO_2$, both the Schmidt number Sc in the k-U_{10} relationship and the solubility s primarily depend on water temperature. The solubility of CO_2 in sea water is estimated using the formula derived by *Weiss* [1974]. For the temperature dependence of the Schmidt number, it is found that a fourth-order polynomial gives best fitting of the data measured by *Jähne et al.* [1987b] with the temperatures ranging from 0°C to 40°C. The variations in temperature result in the opposite effects on the Schmidt number and the solubility of CO_2. This gives rise to a weak temperature dependence on the exchange coefficient $K \equiv k \times s$ [see, e.g., *Etcheto and Merlivat*, 1988].

[16] The surface integration of the local CO_2 flux over the global ice-free ocean surface is discretized by equally dividing the longitude (90°S to 90°N) and the latitude (180°W to 180°E) and approximating the surface by a Hughes rotational ellipsoid.

3. Data

[17] Monthly climatological ΔpCO_2 maps of the global oceans have recently been constructed by *Takahashi et al.* [1997]. The mappings are based on approximately 250,000 field measurements and an interpolation scheme using a lateral two-dimensional transport model developed by *Takahashi et al.* [1995]. Measured data which were taken during the El Ñino period in the area of the equatorial Pacific between 10°N and 10°S were excluded from the data bin. The resolution of the maps is 4° latitude $\times$ 5° longitude.

[18] To obtain the monthly climatological wind speed distributions, wind speeds derived from the radiances measured by the Special Sensor Microwave Imager (SSM/I) instrument on board satellites of the Defense Meteorological Satellite Program (DMSP) using the algorithm of *Wentz* [1997] are employed in the present study. The data set contains wind vectors, pseudo stress vectors, and wind speeds, nominally 10 m above the surface, averaged over 5 days and 0.5 degrees in latitude and longitude, over the global ice-free oceans, between January 1990 and December 1996. The 5-day data are averaged into monthly data for a calendar year. It has been shown by *Boutin and Etcheto* [1991] that in determining the CO_2 exchange coefficient, intrinsic errors may arise from the use of satellite measurements of wind speeds. Such errors are attributed to spatial integration and temporal averaging of the sampled satellite wind speeds. Air-sea exchange coefficient estimated using mean monthly wind speeds tends to be smaller than that using high-frequency wind data with short-term variability [*Bates and Merlivat*, 2001]. These errors, however, are smaller relative to those from other sources [*Boutin and Etcheto*, 1991], such as uncertainties which arise from the parameterization of transfer velocity [*Etcheto et al.*, 1991] and the accuracy of the probability of errors in the satellite wind speeds [*Boutin and Etcheto*, 1990].

[19] The NOAA/NASA AVHRR Oceans Pathfinder "best" sea surface temperature (SST) data [*Vazquez et al.*, 1996] are used. These data were derived from the five-channel Advanced Very High Resolution Radiometer (AVHRR) instrument on board the NOAA -7, -9, -11 and -14 polar orbiting satellites using the NOAA/NASA Pathfinder SST algorithm. The "best" SST data are those that passed the strictest set of test criteria described below. Again, the data cover the period from January 1990 through

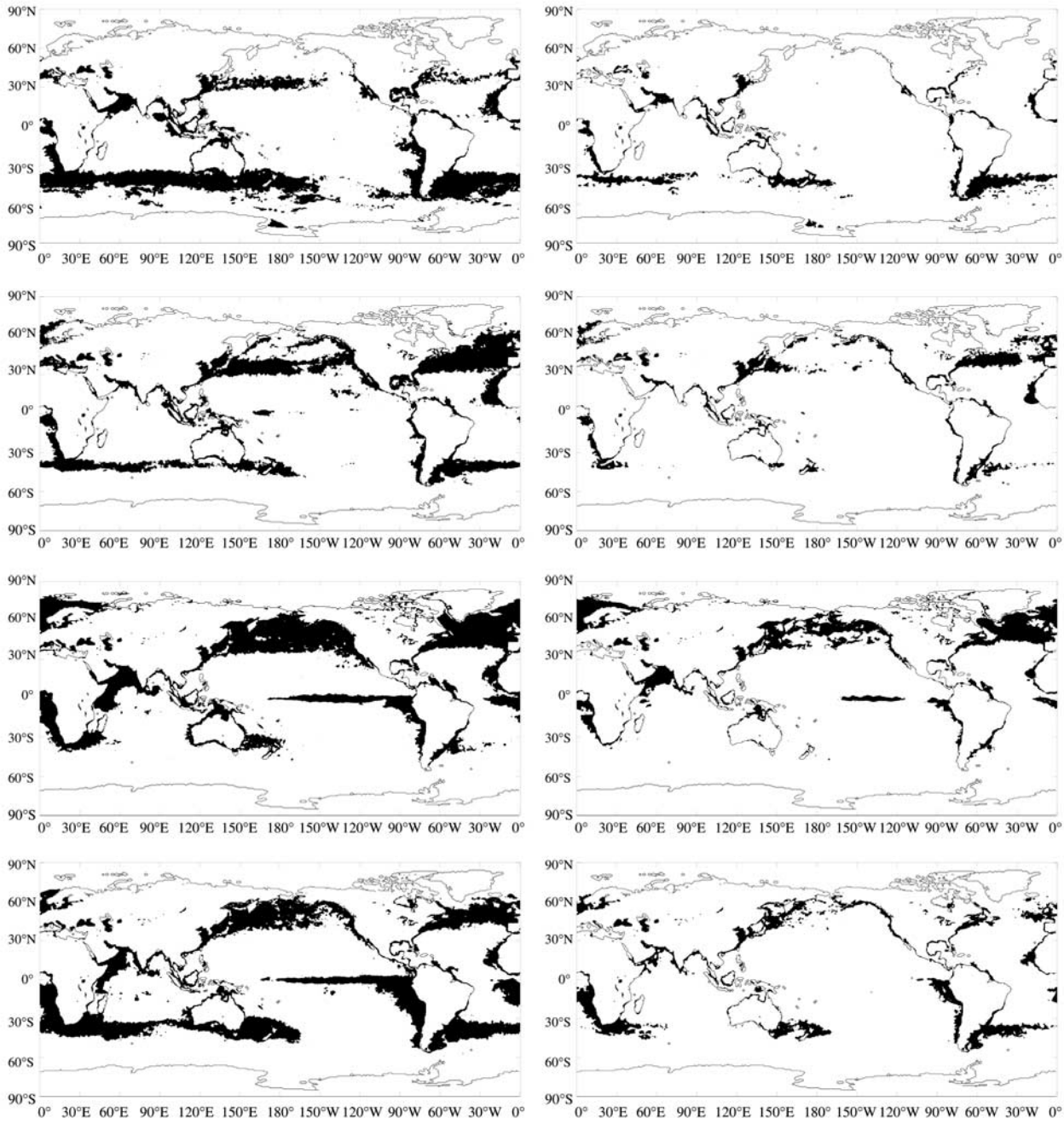

Figure 2. Maps illustrating surfactant coverage of the global oceans for January, April, July, and October. A surface of ocean is considered surfactant-covered when the primary productivity is above a threshold value. In the column on the right, regions with a primary productivity of $PP > 25$ g-C m^{-2} mon^{-1} are defined as surfactant-influenced. In the column on the left, the threshold value which defines surfactant-covered is $PP > 15$ g-C m^{-2} mon^{-1}.

December 1996. Both wind speed and SST data were obtained from the NASA Physical Oceanography Distributed Active Archive Center at the Jet Propulsion Laboratory, California Institute of Technology.

[20] Owing to the absence of global maps of surfactant coverage and the well-known fact that phytoplankton can produce surfactants [e.g., *Frew et al.*, 1990], we use a threshold value of the local primary productivity as an indicator of the presence of surfactants as in *Asher* [1997]. Global ocean primary productivity distribution maps estimated from SeaWIFS ocean color images using the semianalytical model of *Behrenfeld and Falkowski* [1997] are used. The data were provided by the Ocean Primary Productivity Research Team at the Institute of Marine and Coastal Sciences, Rutgers University.

[21] In that the presence of surfactants is estimated by assuming a threshold value of primary productivity, *pp*, the degree of reduction in the global CO_2 flux is dictated by the

chosen threshold value. Three different scenarios of the oceans are considered in the following results and discussions: (1) surfaces which are clean everywhere; (2) surfaces which are considered to be covered with surfactants when $pp > 25$ g-C m^{-2} mon^{-1}; and (3) surfaces which are considered to be covered with surfactants when $pp > 15$ g-C m^{-2} mon^{-1}.

[22] We choose primary production values of 15 and 25 g-C m^{-2} mon^{-1} as the postulated thresholds for the existence of surfactants. The lower threshold value (15 g-C m^{-2} mon^{-1}) is about twice the mean primary production value of the oligotrophic ocean [*Antoine et al.*, 1996]. It is also close to the mean primary production value of the Atlantic Ocean [*Longhurst et al.*, 1995], which is a major CO_2 sink. If the real threshold is indeed as low as this value, the surfactants would affect large areas that show a sizable phytoplankton growth rate. The higher threshold value (25 g-C m^{-2} mon^{-1}) is about midway between the mean primary production values of mesotrophic and eutrophic oceans [*Antoine et al.*, 1996]. This approximates the lower limit of the mean primary production values for the most productive regions, namely, the coastal zones, the upwelling systems, and the polar regions [*Longhurst et al.*, 1995]. On the other hand, if the real threshold is as high as this value, the surfactants would only affect the most productive regions.

[23] Geographical variations in the surfactant coverage of the global oceans for January, April, July, and October are shown in Figure 2 for the two surfactant coverage conditions considered. Depending on the chosen threshold of primary productivity, the area of surfactant coverage varies. In general, the surfaces are practically free of surfactants in the central gyres of oceans. In the Northern Hemisphere the major regions of surfactant distribution are the subarctic Pacific and Atlantic in boreal summer and autumn (between March and September). In the eastern equatorial and subtropical Pacific and Atlantic waters off the coasts of America and Africa, where nutrient-rich water wells up, the surfaces are covered with surfactants in austral spring and summer (between July and December). In the Indian Ocean the Arabian Sea and surface waters off the east coasts of Africa are also covered with surfactants from July to October. The distribution of surfactants in the Southern Ocean begins in July mostly off the west coasts of South Africa, South America, and Australia. The area expands and extends eastward, reaching its maximal surfactant coverage in December and January.

4. Results of CO_2 Exchange Coefficients

[24] Monthly variations in the mean global exchange coefficient, $K \equiv k \times s$, for the three surface conditions of the oceans are shown in Figure 3. For ocean surfaces devoid of surfactant coverage, the global exchange coefficient reaches its maximum in July and December. The calculated annual mean of the exchange coefficient is 3.24×10^{-2} mol m^{-2} yr^{-1} μatm^{-1}. It becomes 3.30×10^{-2} mol m^{-2} yr^{-1} μatm^{-1} when the dependence of solubility and the Schmidt number on the sea surface temperature are ignored, and the temperature is assumed to be 20°C as in the calculations of *Etcheto and Merlivat* [1988] and *Etcheto et al.* [1991]. This is close to 3.34×10^{-2} mol m^{-2} yr^{-1} μatm^{-1} as calculated by *Etcheto et al.* [1991] who also used SSM/I wind speed data. (*Etcheto et al.* [1991] use instantaneous wind speed measurement at 25 km resolution to compute the CO_2 transfer velocity. The transfer velocity is then averaged at 2.5° × 2.5° grid resolution to compute the exchange coefficient.) This finding provides further credence to our calculations.

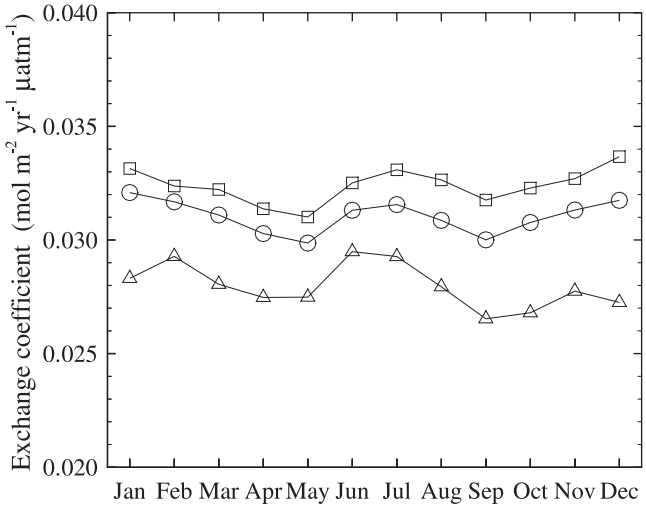

Figure 3. Monthly variations in the global CO_2 exchange coefficient (mol m^{-2} yr^{-1} μatm^{-1}) for the three surface conditions described in Figure 2 (clean oceans (square), oceans which are defined as surfactant-covered when $PP > 25$ g-C m^{-2} mon^{-1} (circle) and those when $PP > 15$ g-C m^{-2} mon^{-1} (triangle).

[25] The degree of reduction caused by the presence of surfactants is mostly constant throughout the seasons for the threshold value of $pp = 25$ g-C m^{-2} mon^{-1}. The annual mean of the global exchange coefficient decreases from 3.24×10^{-2} mol m^{-2} yr^{-1} μatm^{-1} of the clean ocean to 3.10×10^{-2} mol m^{-2} yr^{-1} μatm^{-1}. In the case of the threshold value of $pp = 15$ g-C m^{-2} mon^{-1}, further reduction occurs and the annual mean decreases to 2.80×10^{-2} mol m^{-2} yr^{-1} μatm^{-1} since the area of surfactant coverage increases. The most drastic reduction occurs in boreal winter (austral summer), especially in the months of December and January.

[26] The cause of such a change in the seasonal variability of the global exchange coefficient can be exemplified by examining the effect of surfactants on individual sectors of the global ocean. Accordingly, the global ocean surface is divided into six major sectors: (1) northern (10°N to 70°N) Pacific sector; (2) equatorial and southern (40°S to 10°N) Pacific sector; (3) northern (10°N to 70°N) Atlantic sector; (4) equatorial and southern (40°S to 10°N) Atlantic sector; (5) Indian Ocean sector; and (6) Southern Ocean (south of 40°S) sector. This partitioning is primarily based on the gradient direction of ΔpCO_2 distributions. Annual variations in the exchange coefficient of each ocean sector for the three surface conditions are shown in Figure 4. It is clear that the two maxima of the global exchange coefficient in July and December are attributed to strong austral winter winds in the Southern and Indian sectors and boreal winter winds in the northern Pacific and Atlantic sectors.

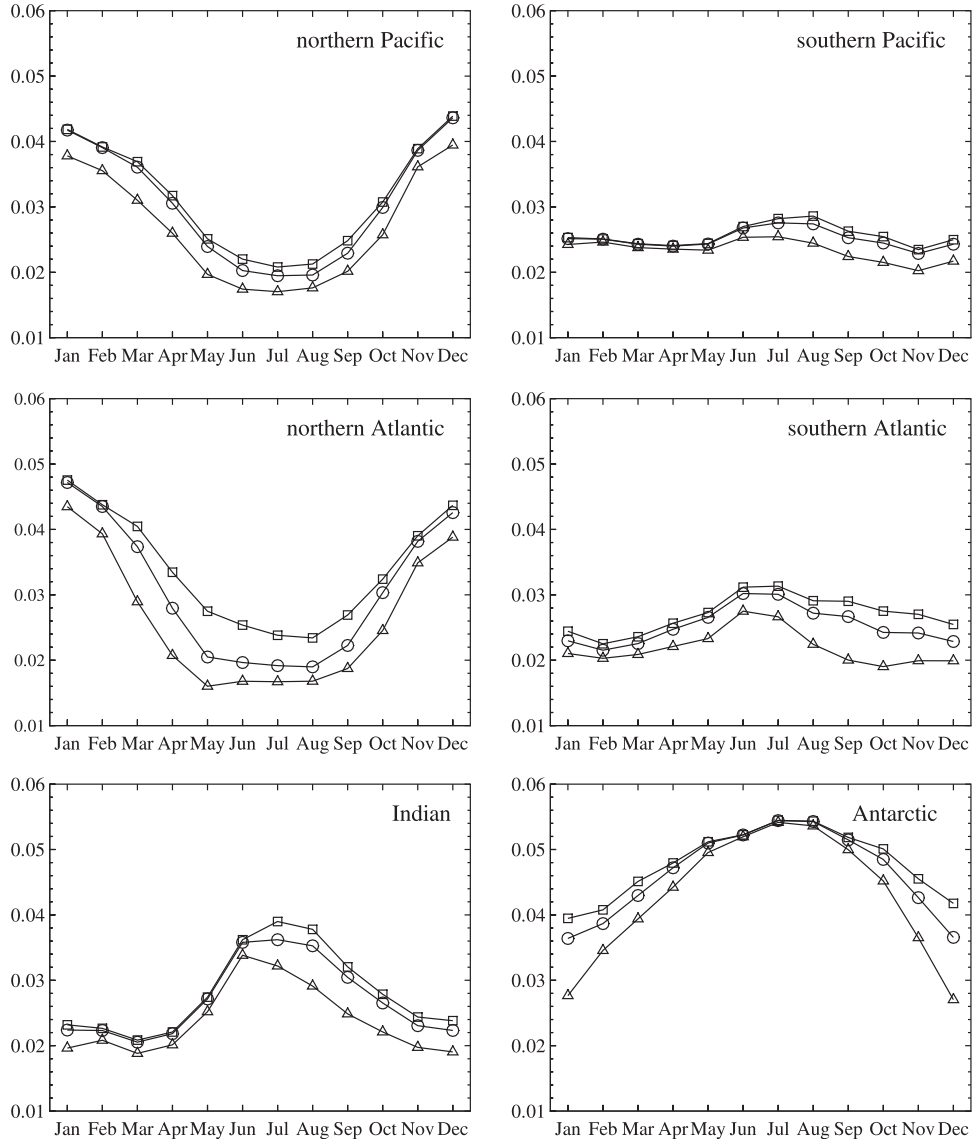

Figure 4. Seasonal variations of the averaged CO_2 exchange coefficient (mol m^{-2} yr^{-1} μatm^{-1}) in various major ocean sectors for the three surface conditions described in Figure 2.

[27] Except in the Indian Ocean, the strong reduction in the CO_2 exchange coefficient by surfactants typically occurs in seasons when the transfer enhancement by wind is weak and vice versa. This feature is particularly pronounced in the Southern Ocean sector. The degree of the surfactant effect on an individual ocean sector is determined by the distributions of both the magnitude of the exchange coefficient and the presence of surfactants. The distribution maps of the CO_2 exchange coefficient reduction by surfactants, showing such combined effect, using the threshold value of pp = 15 g-C m^{-2} mon^{-1} for the months of January, April, July and October are shown in Figure 5.

[28] In the Southern Ocean sector the maximal reduction in the CO_2 exchange coefficient by surfactants occurs between December and January when the exchange coefficient reaches its annual minimum (Figure 4); nevertheless, the area of surfactant coverage is maximal. This results in the strongest surfactant effect found throughout the year. In the months between May and August, when the Westerlies are at their strongest, the situation is reversed. The exchange coefficients in the Southern Ocean sector remain the highest among the global oceans with a factor of nearly 3 higher than in the northern Pacific and Atlantic sectors, but the surfactant effect virtually vanishes. The distribution of the exchange-coefficient reduction (Figure 5) reveals that only a small fraction of the Southern Ocean surface is covered with surfactants from May to August.

[29] The northern Pacific and Atlantic sectors have similar seasonal variabilities as far as the exchange coefficient and the surfactant effect are concerned. The exchange coefficients in the Atlantic, however, are reduced much more significantly by the presence of surfactants than they are in the Pacific (Figure 4), particularly in the case of a higher threshold value (pp = 25 g-C m^{-2} mon^{-1}). In the Northern Hemisphere the strong seasonal variations of the Westerlies between 30°N and 60°N in the northern Pacific and Atlantic lead to an abrupt drop in the exchange coefficient from the highest values in boreal winter (between December and

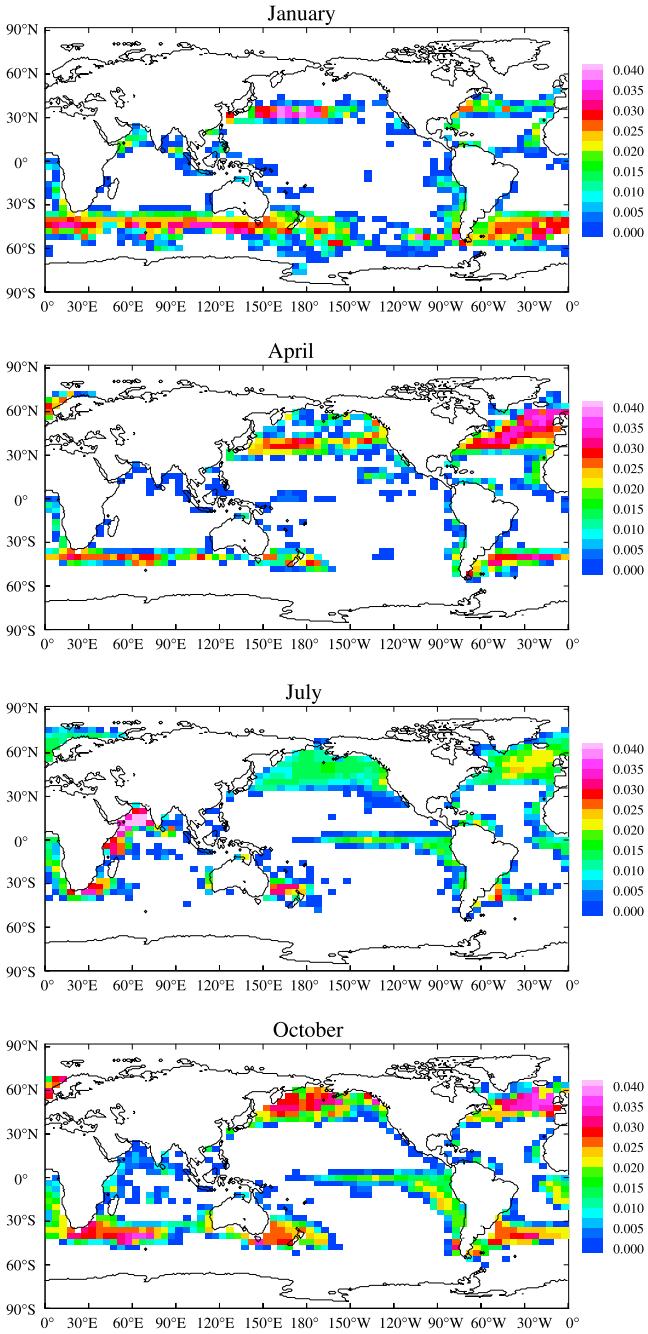

Figure 5. Maps of CO_2 exchange coefficient reduction in units of mol m^{-2} yr^{-1} μatm^{-1} by surfactants using the threshold value of pp = 15 g-C m^{-2} mon^{-1} for the months of January, April, July, and October. Blank areas of the oceans are free of surfactants, and therefore no reduction in the exchange coefficient is found.

January) to the lowest values in summer. Meanwhile, the surfactant coverage in both the northern Pacific and Atlantic sectors expands from the minimum in boreal winter to the annual maximum in summer. This further reduces the exchange coefficients of the northern Pacific and Atlantic Oceans in boreal summer to values which are the lowest among all in the global oceans.

[30] In the Indian Ocean sector the strong winds in summer (between June and August) during the Southwest Monsoon intensify CO_2 transfer and result in annual maximal exchange coefficients. In the same period, the CO_2 exchange coefficients of the Indian Ocean sector are higher than those of the equatorial and southern Pacific and Atlantic sectors. In contrast to other sectors of the global oceans, in the Indian Ocean dominant surfactant effects occur in seasons with high exchange coefficients. The reason for such a seasonal pattern is that the Arabian Sea, where the surface winds are strong, is covered by surfactants during the Southwest Monsoon period. This results in a large area with a high degree of reduction in the exchange coefficient for the months of June, July, and August, as shown in Figure 5.

[31] Seasonal variations of the exchange coefficient in the equatorial and southern Pacific and Atlantic are similar to but weaker than those in the Indian Ocean sector. In the austral autumn and winter (between January and June) the surfactant effect virtually vanishes in the equatorial and southern Pacific. The major coverage of surfactants occurs in the eastern equatorial and subtropical water off the coasts of southern America and Africa in the austral spring and summer. The local wind-enhanced gas exchange and, consequently, the degree of reduction in the exchange coefficient in these areas is less than the corresponding value for other sectors of the global oceans during the same period, as shown in Figure 5.

5. Results of CO_2 Fluxes

[32] The discussion on the exchange coefficient in the previous section does not take into consideration the direction of the exchange flux, which depends on the sign of the ΔpCO_2 gradient. The geographical and seasonal variations in the CO_2 fluxes over the global oceans are further

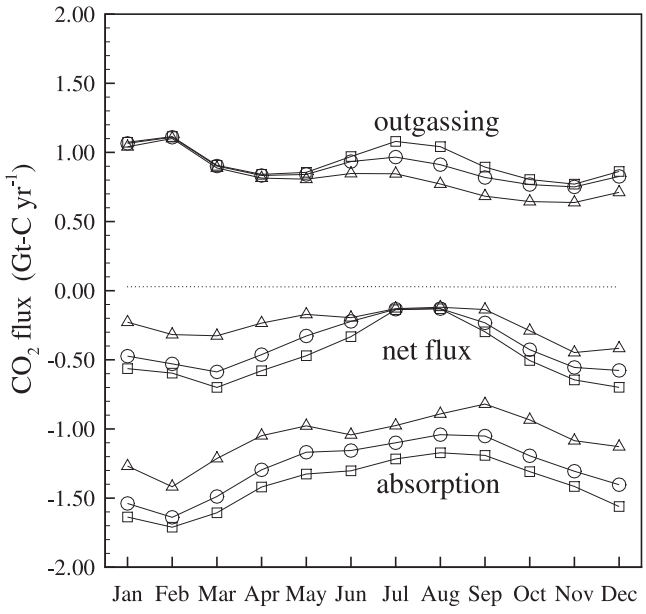

Figure 6. Seasonal variations of the global CO_2 net, outgassing, and absorption fluxes (Gt-C yr^{-1}) for the three surface conditions (clean oceans (square), oceans which are defined as surfactant-covered when PP > 25 g-C m^{-2} mon^{-1} (circle), and those when PP > 15 g-C m^{-2} mon^{-1} (triangle) described in Figure 2.

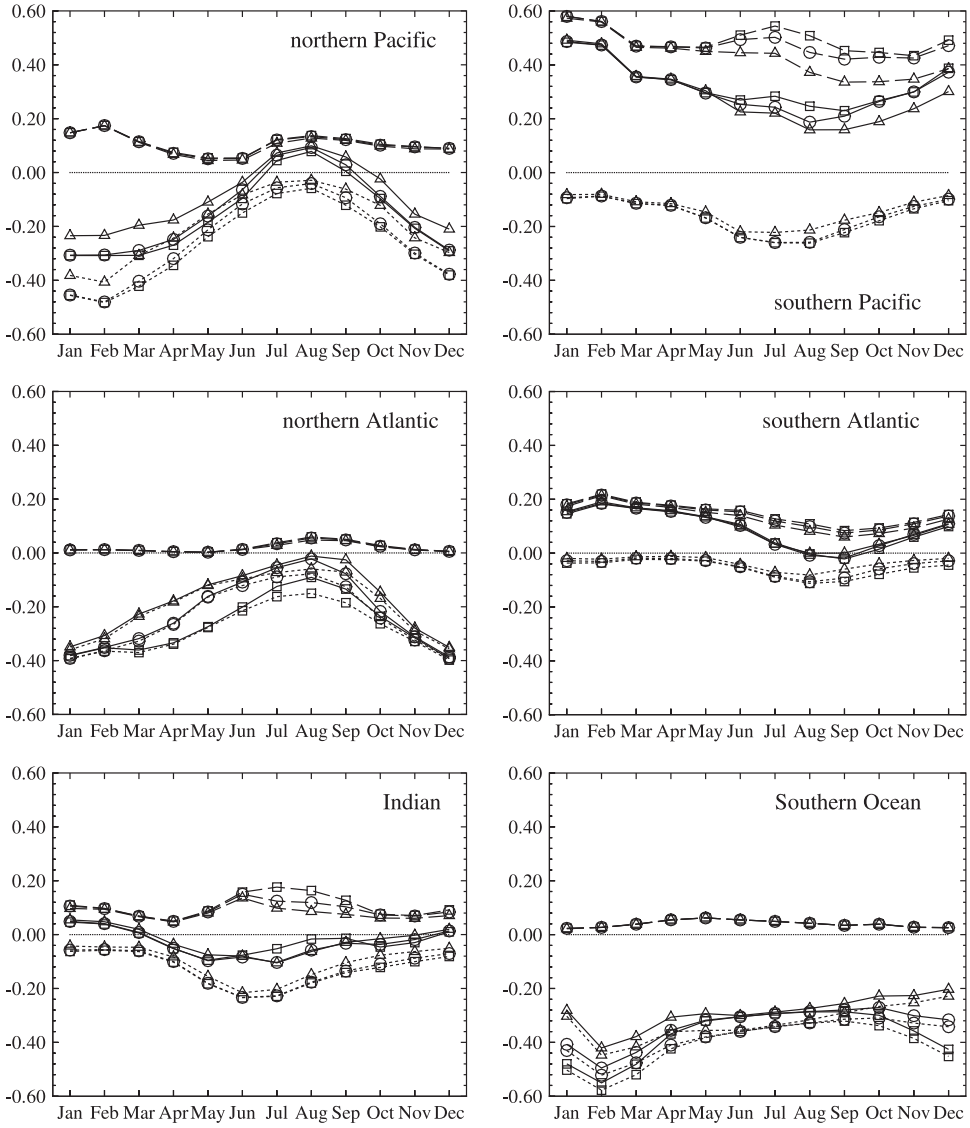

Figure 7. Seasonal variations of the CO_2 net (solid curve), outgassing (long-dashed curve) and absorption (short-dashed curve) fluxes (Gt-C yr^{-1}) in various major ocean sectors for the three surface conditions (clean oceans (square), oceans which are defined as surfactant-covered when $PP > 25$ g-C m^{-2} mon^{-1} (circle), and those when $PP > 15$ g-C m^{-2} mon^{-1} (triangle) described in Figure 2.

complicated by the distributions of both the magnitude and direction of CO_2 partial-pressure gradients across the atmosphere-ocean interface. Monthly variations of the global CO_2 net fluxes as well as outgassing (from ocean to atmosphere) and absorption (from atmosphere to ocean) fluxes for the three scenarios of surface conditions considered are shown in Figure 6. To reveal the geographical variability of the surfactant effect, the seasonal variations in the CO_2 fluxes of the major ocean sectors for the three surface conditions are plotted in Figure 7. In all cases, the net global CO_2 transfer is downward throughout the year.

5.1. Fluxes Without Surfactant Coverage

[33] In the case of the surfactant free global oceans, the net CO_2 flux ranges from -0.70 Gt-C yr^{-1} (-1.20 Gt-C yr^{-1} using k_W) in December to -0.13 Gt-C yr^{-1} (-0.23 Gt-C yr^{-1} using k_W) in August (Figure 6). The maxima of both outgassing and absorption fluxes occur in February with values of 1.11 Gt-C yr^{-1} and -1.71 Gt-C yr^{-1}, (1.81 Gt-C yr^{-1} and -2.80 Gt-C yr^{-1} using k_W), respectively. The least outgassing occurs in November with a value of 0.77 Gt-C yr^{-1}, (1.25 Gt-C yr^{-1} using k_W), whereas the least absorption occurs in August with a value of -1.17 Gt-C yr^{-1} (-1.91 Gt-C yr^{-1} using k_W). Resolving the global net flux by geographical sectors, the major uptake occurs in the Southern Ocean sector throughout the year and in the northern Pacific and Atlantic sectors in boreal winter and spring from November to April (Figure 7). The southern Pacific is the strongest source of CO_2 year round with the maximal release occurring in January.

[34] A comparison between the zonal oceanic annual CO_2 fluxes estimated in the present study using SSM/I satellite wind data and the calculations of *Takahashi et al.* [1997] using the climatological wind field of *Esbensen and Kush-*

nir [1981] is shown Figure 8 in 4° wide latitude bands. The most notable difference between the two calculations occurs in the tropical region (14°S to 4°N) where the present estimate of upward CO_2 flux is higher than that of *Takahashi et al.* [1997]. Over the northern and southern temperate regions the present calculations of downward CO_2 flux, however, are slightly lower. Such a discrepancy in the estimated CO_2 fluxes is attributed to the different wind fields used in the calculations. Also plotted in Figure 8 are the corresponding distributions of the longitudinal-averaged annual ΔpCO_2 and the wind fields of *Esbensen and Kushnir* [1981] and SSM/I. Over the low-latitude tropical oceans (between 20°S and 20°N), where CO_2 fluxes are upward, the windspeed values of SSM/I are higher than those of *Esbensen and Kushnir* [1981]. By contrast, in the northern and southern temperate regions, where the average fluxes are downward, the SSM/I wind field gives lower average windspeeds than those of Esbensen and Kushnir. As a consequence, such a difference in the wind fields results in lower net global flux in the present calculation than that estimated by *Takahashi et al.* [1997].

[35] Using ΔpCO_2 maps compiled with the objective mapping technique, *Lefèvre et al.* [1999] estimated the CO_2 fluxes for the northern Pacific and Atlantic Oceans. The comparison of the seasonal CO_2 fluxes for the Pacific and Atlantic north of 10°S computed by *Lefèvre et al.* [1999] and in this study using the ΔpCO_2 maps of *Takahashi et al.* [1997] incorporating a lateral diffusion-advection numerical scheme [*Takahashi et al.*, 1995] is shown in Table 1. SSM/I satellite wind fields and, for comparison, the formulations of the gas transfer velocity by *Liss and Merlivat* [1986] (k_L) and *Wanninkhof et al.* [1992] (k_W) are used in both calculations. A similar comparison was also made by *Lefèvre et al.* [1999]. In their calculations, all the observed ΔpCO_2 values were assumed to be independent of the year of measurements. In the present calculation, however, integrated CO_2 fluxes using two sets of ΔpCO_2 values given by *Takahashi et al.* [1997] (denoted by $\Delta pCO_2|_{dp}$ and $\Delta pCO_2|_{hf}$, which employ "full" and "half" schemes to normalize the observed ΔpCO_2 to a reference year) are included for comparison. The correction from the ΔpCO_2 data of *Takahashi et al.* [1997] is not removed in this study as it was in the study by *Lefèvre et al.* [1999]. Despite this, the CO_2 fluxes computed in both studies, using the same wind fields but different ΔpCO_2 maps constructed with different interpolation schemes, compare well for both the Atlantic and Pacific Oceans. The CO_2 fluxes computed on the basis of the ΔpCO_2 data of *Takahashi et al.* [1997] are mostly within the range of uncertainty of the estimated fluxes by *Lefèvre et al.* [1999], except in the tropic Atlantic (10°S ~ 10°N) for all four quarters of the year, in the subarctic Atlantic (50°N ~ 80°N) for the third quarter (July to September) and in the subarctic Pacific (50°N ~ 65°N) for the third quarter. However, as noted by *Lefèvre et al.* [1999] and many others, the errors in estimating the CO_2 fluxes caused by the large uncertainty in the gas transfer coefficient k may exceed those attributed to insufficient ΔpCO_2 data. Such errors are further complicated by seasonal and geographical variations in the surfactant distributions.

5.2. Fluxes Considering Surfactant Coverage

[36] As shown in Figure 6, the distribution of surfactants over the global oceans reduces the monthly CO_2 net flux

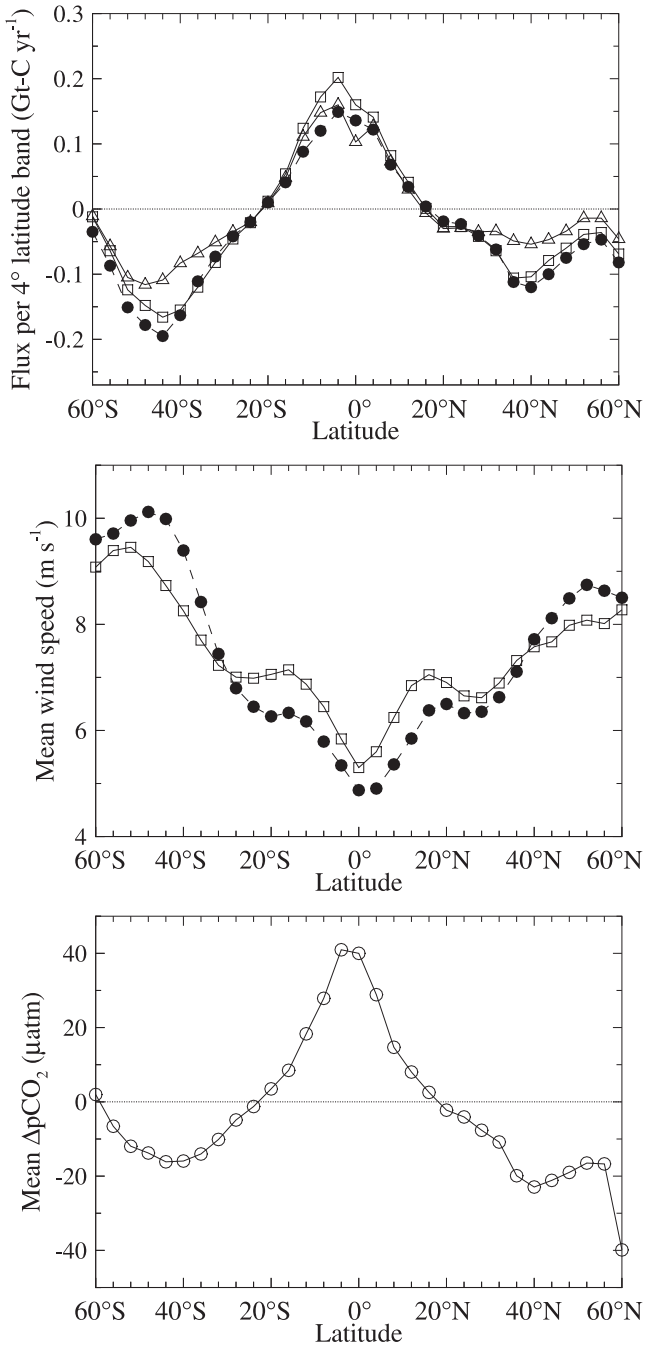

Figure 8. Comparison of zonal oceanic annual CO_2 fluxes (Gt-C yr^{-1}) estimated in the present study (square in the top panel) using SSM/I satellite wind data (square in the middle panel) with the calculations of *Takahashi et al.* [1997] using the climatological (small circle in the top panel) wind field of *Esbensen and Kushnir* [1981] (small circle in the middle panel) depicted in 4° wide latitude bands. Both calculations use the transfer velocity formulated by *Wanninkhof* [1992] (k_W) and ΔpCO_2 values applying full atmospheric CO_2 increase normalization scheme (bottom panel). Also shown in the figure is the distribution of zonal fluxes considering the influence of surfactants with the surfactant coverage condition of $pp > 15$ g-C m^{-2} mon^{-1} (triangle in the top panel).

Table 1a. Comparison of the Computed CO_2 Flux in the Northern Atlantic Ocean (Between 80°W and 10°E) in the Present Study With That Given by *Lefèvre et al.* [1999] Using Two Gas Transfer Velocities k_W [*Wanninkhof*, 1992] and k_L [*Liss and Merlivat*, 1986][a]

Seasonal Period	Latitudinal Band	Results of *Lefèvre et al.* [1999]		Present Results Using $\Delta pCO_2\|_{dp}$		Present Results Using $\Delta pCO_2\|_{hf}$	
		Flux, k_L	Flux, k_W	Flux, k_L	Flux, k_W	Flux, k_L	Flux, k_W
January to March	10°S–10°N	0.12 ± 0.03	0.21 ± 0.05	0.068	0.111	0.068	0.111
	10°N–50°N	−0.24 ± 0.08	−0.39 ± 0.15	−0.255	−0.420	−0.251	−0.412
	50°N–80°N	−0.12 ± 0.05	−0.20 ± 0.10	−0.109	−0.196	−0.093	−0.167
April to June	10°S–10°N	0.06 ± 0.05	0.11 ± 0.09	0.055	0.088	0.054	0.088
	10°N–50°N	−0.14 ± 0.07	−0.22 ± 0.12	−0.180	−0.284	−0.179	−0.282
	50°N–80°N	N/A	N/A	−0.088	−0.140	−0.081	−0.129
July to September	10°S–10°N	0.06 ± 0.04	0.11 ± 0.08	0.051	0.082	0.051	0.082
	10°N–50°N	0.06 ± 0.07	0.12 ± 0.12	−0.003	−0.003	−0.0006	0.0004
	50°N–80°N	−0.17 ± 0.02	−0.26 ± 0.03	−0.113	−0.178	−0.105	−0.167
October to December	10°S–10°N	0.05 ± 0.02	0.10 ± 0.05	0.069	0.109	0.069	0.109
	10°N–50°N	−0.12 ± 0.08	−0.18 ± 0.14	−0.158	−0.259	−0.152	−0.250
	50°N–80°N	N/A	N/A	−0.157	−0.267	−0.142	−0.242

[a] $\Delta pCO_2|_{dp}$ and $\Delta pCO_2|_{hf}$ denote two sets of ΔpCO_2 values given by *Takahashi et al.* [1997] which employ "full" and "half" schemes, respectively, to normalize the observed ΔpCO_2 to a reference year.

except in the period between July and August, during which time the gross surfactant effect virtually vanishes. The maximal reduction in the net flux occurs in boreal spring (between January and April). Resolving the net flux into outgassing and absorption components, however, reveals interesting features in seasonal variability of the surfactant effect. For almost half of the year (between January and May) the presence of surfactants does not affect CO_2 outgassing from global oceans. This indicates that the fractional areas of the global ocean surface, across which the CO_2 gradients are positive, are almost free of surfactants (or are low in biological activities according to our definition of surfactant coverage) in boreal spring and summer. Unlike the findings for outgassing, CO_2 uptake by the oceans is suppressed by the presence of surfactants throughout the year. In boreal spring the distribution of surfactants has a negligible effect on CO_2 outgassing transfer, which results in maximal net flux reduction. In the period between July and August the reduction in absorption transfer is balanced by a compatible reduction in outgassing, and the resultant net flux is unaffected by the presence of surfactants. In fact, the surfactant effect is prominent in this period.

[37] A comparison of the compound effect of surfactants on the global annual CO_2 flux for two distribution conditions is shown in Table 2. The average reduction percentage of absorption transfer by surfactants is about twice that of outgassing for both surfactant coverage conditions. This means that the presence of surfactants suppresses the uptake of CO_2 by the ocean to a greater degree than it does the release of CO_2 to the atmosphere. To provide further evidence of such an asymmetric surfactant effect, zonal profiles of annual CO_2 fluxes across both clean and surfactant-influenced (coverage condition $pp > 15$ g-C m^{-2} mon^{-1}) global oceans are shown in Figure 8. Reductions in the uptake fluxes over the southern and northern temperate zones are more significant than the decrease in outgassing flux in the equatorial band. On global average the annual net CO_2 flux is reduced by approximately 20% with the surfactant coverage condition of $pp > 25$ g-C m^{-2} mon^{-1} and about 50% (ranging from 47% to 58% depending on the transfer velocity and the ΔpCO_2 map used) with the condition of $pp > 15$ g-C m^{-2} mon^{-1}.

[38] In the northern Pacific and Atlantic sectors the surfactant effect is primarily on suppressing absorption transfer (see Figure 7). Such reduction continues throughout

Table 1b. Comparison of the Computed CO_2 Flux in the Northern Pacific Ocean (Between 80°W and 10°E) in the Present Study With That Given by *Lefèvre et al.* [1999] Using Two Gas Transfer Velocities k_W [*Wanninkhof*, 1992] and k_L [*Liss and Merlivat*, 1986][a]

Seasonal Period	Latitudinal Band	Results of *Lefèvre et al.* [1999]		Present Results Using $\Delta pCO_2\|_{dp}$		Present Results Using $\Delta pCO_2\|_{hf}$	
		Flux, k_L	Flux, k_W	Flux, k_L	Flux, k_W	Flux, k_L	Flux, k_W
January to March	15°S–15°N	0.32 ± 0.17	0.58 ± 0.29	0.418	0.674	0.417	0.672
	15°N–50°N	−0.34 ± 0.33	−0.55 ± 0.54	−0.340	−0.558	−0.329	−0.539
	50°N–65°N	0.12 ± 0.06	0.20 ± 0.10	0.061	0.103	0.067	0.115
April to June	15°S–15°N	0.45 ± 0.20	0.81 ± 0.36	0.385	0.642	0.384	0.641
	15°N–50°N	−0.33 ± 0.15	−0.52 ± 0.23	−0.189	−0.297	−0.183	−0.286
	50°N–65°N	−0.013 ± 0.04	−0.02 ± 0.06	0.003	0.004	0.007	0.011
July to September	15°S–15°N	0.32 ± 0.22	0.56 ± 0.38	0.423	0.678	0.421	0.676
	15°N–50°N	0.04 ± 0.11	0.07 ± 0.19	0.041	0.068	0.048	0.078
	50°N–65°N	−0.05 ± 0.02	−0.08 ± 0.03	−0.024	−0.038	−0.020	−0.032
October to December	15°S–15°N	N/A	N/A	0.394	0.633	0.392	0.630
	15°N–50°N	N/A	N/A	−0.188	−0.313	−0.170	−0.283
	50°N–65°N	N/A	N/A	−0.029	−0.048	−0.020	−0.032

[a] $\Delta pCO_2|_{dp}$ and $\Delta pCO_2|_{hf}$ denote two sets of ΔpCO_2 values given by *Takahashi et al.* [1997] which employ "full" and "half" schemes, respectively, to normalize the observed ΔpCO_2 to a reference year.

Table 2a. Comparison of Global Annual CO_2 Flux (Gt-C yr^{-1}) for Clean Global Oceans and Oceans Which are Taken as Covered With Surfactants When $pp > 25$ g-C m^{-2} mon^{-1} Using Two ΔpCO_2 Maps Given by *Takahashi et al.* [1997] and Two Gas Transfer Velocities k_W [*Wanninkhof*, 1992] and k_L [*Liss and Merlivat*, 1986][a]

	k_L			k_W		
Scenario	Net Flux	Outgassing	Absorption	Net Flux	Outgassing	Absorption
Clean	−0.471	0.934	−1.405	−0.772	1.522	−2.294
Case 1	−0.388 (18%)	0.894 (4%)	−1.282 (9%)	−0.624 (19%)	1.445 (5%)	−2.069 (10%)
Case 2	−0.251 (47%)	0.816 (13%)	−1.067 (24%)	−0.373 (52%)	1.301 (15%)	−1.674 (27%)

[a]The percentages in parentheses represent the reduction rates.

the year in the northern Pacific and Atlantic. To further reveal the geographical variability in the surfactant effect, the distribution maps of CO_2 flux reduction by surfactants using the threshold value of $pp = 15$ g-C m^{-2} mon^{-1} are shown in Figure 9 for the months of January, April, July, and October. As shown previously in Figure 5, the major area of surfactant distribution in the Northern Hemisphere is north of 30°N in the Pacific and Atlantic where the wind-enhanced exchange coefficients are high. In particular the major reduction of CO_2 uptake occurs along the latitudinal band between 30°N and 50°N in the northwestern Pacific and Atlantic regions from March to May.

[39] The equatorial and southern Pacific sector is a major CO_2 source throughout the year (Figure 7). The presence of surfactants effectively suppresses the outgassing flux in austral spring and summer (between July and December) and hence the positive net flux. In contrast to the northern Pacific and Atlantic, where the magnitudes of flux reduction by surfactants remain finite values throughout the year, the equatorial and southern Pacific is unaffected by surfactants for almost half of the year (from January to May). Examining the maps of surfactant coverage of the global oceans (Figure 2) it is seen that there are few biological activities in the Southern Hemisphere, including the southern Pacific and Atlantic sectors and the Indian Ocean in the period between January and May. The most pronounced surfactant effect in the equatorial and southern Pacific occurs in the eastern equatorial and subtropical waters in the period of austral spring and summer owing to the highly productive surface waters off the southern American coast. High positive ΔpCO_2 gradient distribution results in strong CO_2 release and, as a result, large outgassing reduction in this region, although the degree of reduction in the wind-enhanced transfer rate is not high (Figure 9). Such pronounced surfactant effects, however, are absent in austral autumn and winter, and the eastern equatorial and subtropical Pacific waters remain as a strong CO_2 outgassing source.

[40] In the equatorial and southern Atlantic sector the surfactant effect is not as significant as that in the same latitudes of the Pacific. The decrease in outgassing flux is compensated by the reduction in absorption flux, and the seasonal variations in the resulting net CO_2 flux in the southern Atlantic is only slightly influenced by the presence of surfactants.

[41] The Southern Ocean sector is another major CO_2 sink among the sectors considered here. Intense biological activities in austral spring and summer, which virtually vanish in fall and winter, result in strong seasonal variability in the exchange coefficient (Figure 4) and therefore in the absorption flux (Figure 7). As shown in Figure 2, the coverage of the surfactants extends almost all over the entire Southern Ocean sector in January (as it does in November and December). This ensues a significant magnitude of reduction in CO_2 uptake by the Southern Ocean sector in austral spring and summer.

[42] The Indian Ocean is the only sector among the global oceans in which the degrees of CO_2 outgassing and absorption are comparable. As indicated in Figure 5, the major surfactant effects occur in the Arabian Sea and the surface waters off the eastern coast of Africa and result in the strong suppression of outgassing flux from July to September (Figures 7 and 9). Similar to the trend in the equatorial and southern Pacific sector, in the Indian Ocean the reduction of CO_2 outgassing exceeds absorption from July to September. The total decrease in CO_2 release from the equatorial and southern Pacific and Indian Oceans by the presence of surfactants, however, is still lower than the reduction in CO_2 absorption by the other ocean sectors.

[43] *Takahashi et al.* [1999] recently updated the monthly distributions of ΔpCO_2 based on improved observational data and the increase in atmospheric pCO_2 from the reference year of 1990 to 1995. The major difference in the estimates of CO_2 flux using the two ΔpCO_2 occurs in the South Ocean (south of 50°S) and the South Indian Ocean (14°S to 50°S) where the increase in atmospheric pCO_2

Table 2b. Comparison of Global Annual CO_2 Flux (Gt-C yr^{-1}) for Clean Global Oceans and Oceans Which are Taken as Covered With Surfactants When $pp > 15$ g-C m^{-2} mon^{-1} Using Two ΔpCO_2 Maps Given by *Takahashi et al.* [1997] and Two Gas Transfer Velocities k_W [*Wanninkhof*, 1992] and k_L [*Liss and Merlivat*, 1986][a]

	k_L			k_W		
Scenario	Net Flux	Outgassing	Absorption	Net Flux	Outgassing	Absorption
Clean	−0.396	0.943	−1.339	−0.647	1.536	−2.183
Case 1	−0.319 (20%)	0.902 (4%)	−1.221 (9%)	−0.509 (21%)	1.459 (5%)	−1.968 (10%)
Case 2	−0.190 (52%)	0.834 (12%)	−1.014 (24%)	−0.274 (58%)	1.314 (15%)	−1.588 (27%)

[a]The percentages in parentheses represent the reduction rates.

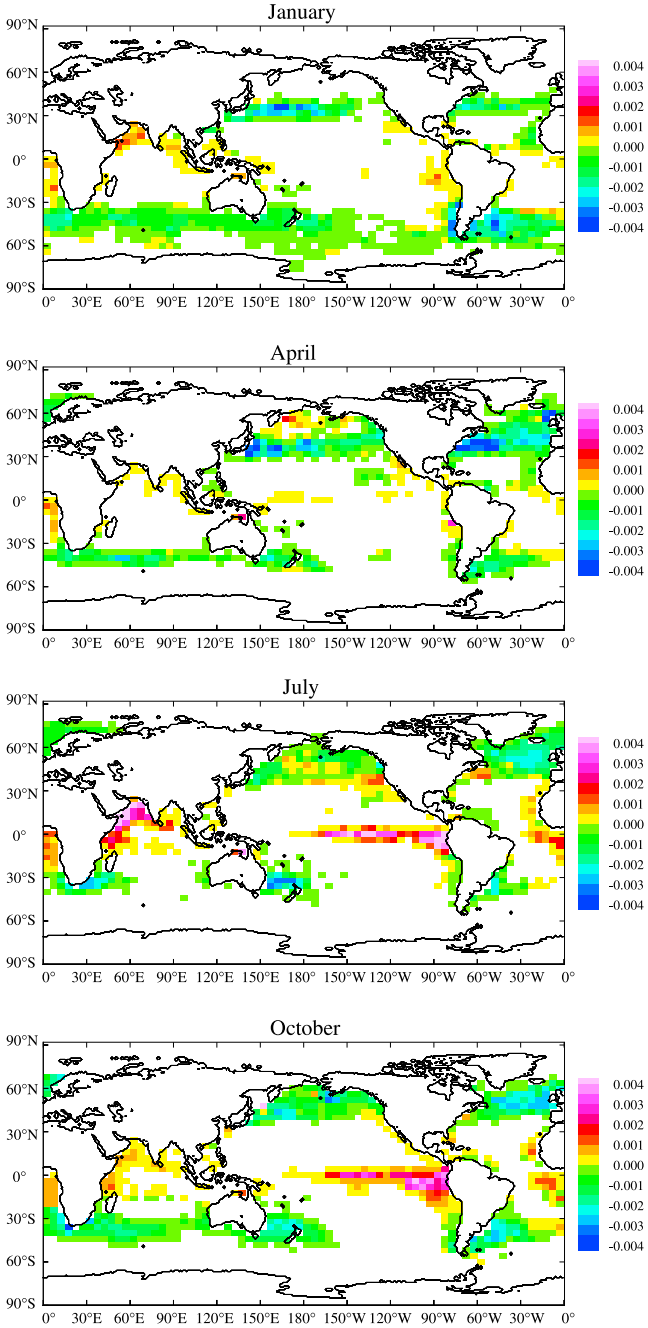

Figure 9. Distribution maps of CO_2 flux reduction in units of Gt-C yr^{-1} by surfactants using the threshold value of pp = 15 g-C m^{-2} mon^{-1} for the months of January, April, July, and October. The negative/positive distribution in the map represents reduction in absorption/outgassing flux. Blank areas of the oceans are free of surfactants, and therefore no reduction in CO_2 flux is found.

causes a -7 μatm change in ΔpCO_2. Over the southern high latitude oceans (south of 50°S), the surfactant effect virtually vanishes which is attributed to the low primary productivity waters there (Figure 2). In this region, the increase in the estimate of CO_2 uptake based on the updated ΔpCO_2 field therefore is not affected by the influence of surfactants. As for the southern Indian Ocean between 14°S and 50°S, high primary productivity waters in austral summer and autumn can cause a significant surfactant effect on CO_2 transfer. Thus the increase in CO_2 uptake associated with the updated ΔpCO_2 in this region is suppressed.

5.3. Probability Distribution of Wind Speeds

[44] To further elucidate the impact of surfactant coverage on global CO_2 fluxes, the probability density functions of wind speeds over the global oceans under the conditions of both positive and negative ΔpCO_2 respectively weighted by the outgassing and absorption fluxes are shown in Figure 10 for the months of January, April, July, and October and the scenario of pp > 15 g-C m^{-2} mon^{-1}. The conditional density functions are obtained by weighting each count of wind speed with the corresponding CO_2 outgassing/absorption flux, which means the integration of the density functions yields the global outgassing/absorption fluxes. The weighted density functions are then normalized by the global outgassing/absorption fluxes. The magnitude of the conditional density function represents the contribution of each possible value of wind speed to the outgassing/absorption flux. The fractional magnitudes reduced by the presence of surfactants are also plotted.

[45] From the distributions of the flux density functions it is clear that the major CO_2 exchange across the ocean surface is contributed by winds with velocities ranging from approximately 5 to 10 m s^{-1}. The cumulative distribution functions, which are also plotted in Figure 10, reveal that CO_2 absorption by the oceans is more likely to occur than outgassing in the high wind range throughout the year. Approximately 90% of the upward CO_2 fluxes occur in regions with wind speeds below 9 m s^{-1}. Similarly, 90% of the downward CO_2 fluxes take place in regions with wind speeds lower than 10 m s^{-1}, except in the months of December, January, and February when the predominant upper limits of wind speed are slightly above 10 m s^{-1}.

[46] The distributions of the fractional densities associated with the reduction of CO_2 transfer by the presence of surfactants also cluster within such an intermediate wind speed range of 5 to 10 m s^{-1}. Nevertheless, drastic seasonal variabilities are observed in the distributions of wind speeds associated with reduced fluxes, particularly outgassing fluxes, in the presence of surfactants. For the outgassing transfer the histograms of wind speed associated with surfactant reduction virtually vanish in the months from January to May, as shown in Figure 6. The two cumulative distributions associated with outgassing and absorption reductions, on the other hand, closely coincide in July and August. This indicates that during this period, in addition to the magnitudes of reduced fluxes, the probability distributions of the wind fields which contribute to outgassing and absorption reductions by surfactants are also similar. However, the two distributions lose their similarity in boreal winter when the magnitude of reduced downward flux increases to its yearly maximum in December. Such strong seasonal variabilities in the distributions of wind speeds associated with reduced fluxes justify the need to consider the effect of surfactants in estimating meaningful global CO_2 flux.

6. Concluding Remarks

[47] In this study we conduct an assessment of the effect of naturally occurring surfactants on the direct calculation of the

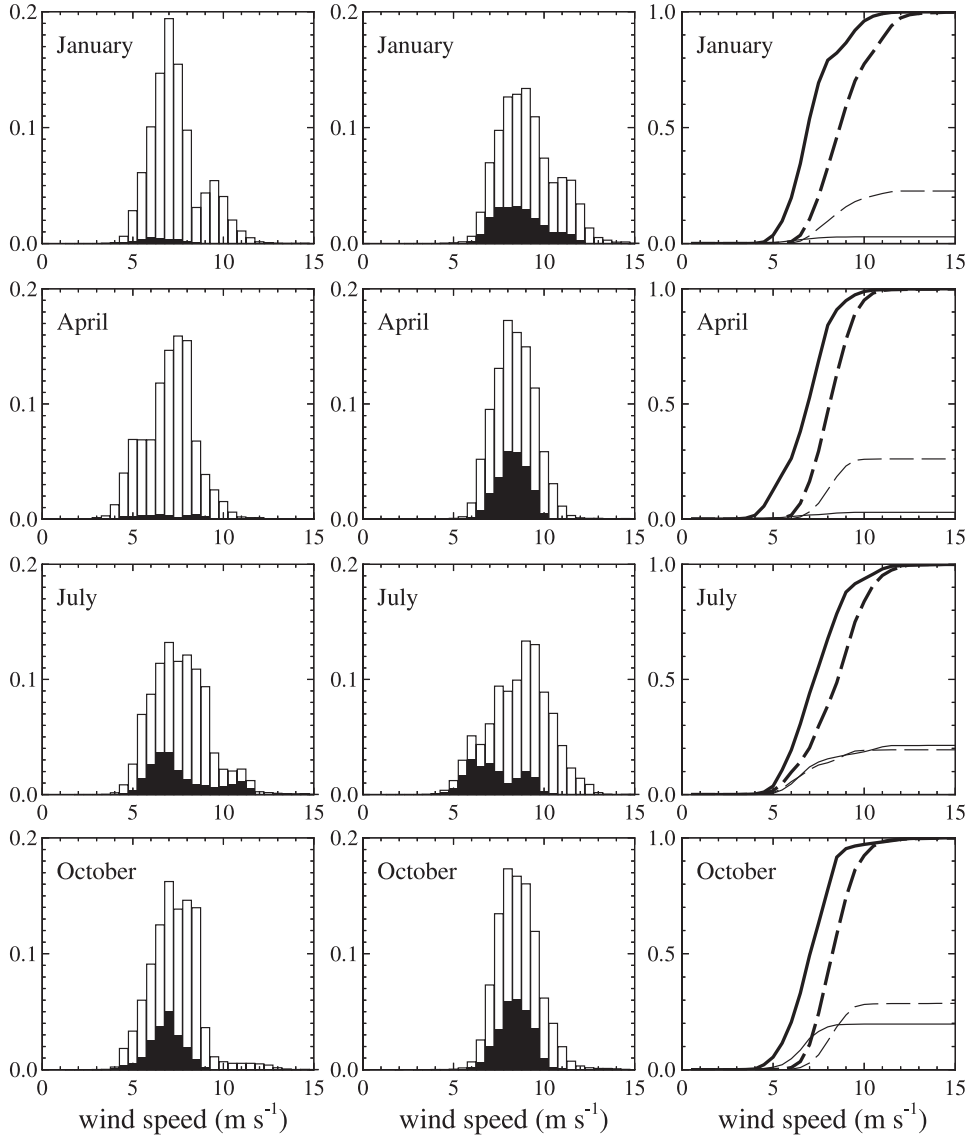

Figure 10. Normalized probability density functions of the wind speeds over the global oceans under the conditions of positive (left column) and negative (central column) ΔpCO_2 weighted respectively by the outgassing and absorption fluxes for the months of January, April, July, and October. The fractional magnitudes reduced by the presence of surfactants for the scenario of $pp > 15$ g-C m^{-2} mon^{-1} are indicated by solid bars. The corresponding cumulative distribution functions are shown in the column on the right for the wind speeds contributing to outgassing (solid thick curves) and absorption (dashed thick curves) fluxes and the wind speeds associated with reduced outgassing (solid thin curves) and absorption (dashed thin curves) fluxes by the presence of surfactants.

global CO_2 flux across the ocean surfaces. Although the calculations are based on a simplified model that the presence of surfactants is determined by a threshold of the biological activity and the reduction rate of transfer velocity is a function of the presence of surfactants and the wind speed, the calculated results exhibit noticeable variations and complexities in global CO_2 flux. The complexities are primarily attributed to the interplay between distributions of the surfactant coverage and the directions of the ΔpCO_2 gradients.

[48] Specifically, our calculations indicate that the presence of surfactants suppresses more downward global CO_2 flux than upward flux. This does not result from the gas exchange processes but rather from the natural correlation between the negative ΔpCO_2 and high primary productivity or surfactant coverage. Such asymmetry in flux reductions by surfactants is particularly prevalent in the high latitude regions of the northern Atlantic and Pacific, the major CO_2 sinks among the global oceans. In these regions the high negative ΔpCO_2 distributions are associated with high biological activity, which results in strong oceanic CO_2 undersaturations. On the other hand, high biological productivity also denotes the possibility that these regions are covered with surfactants as suggested by various observations. Concurrent measurements of ΔpCO_2 distributions,

the biological activity, such as chlorophyll *a* concentrations, and ocean-atmosphere CO_2 fluxes would contribute to our understanding of the possible correlations, both positive and negative, among these variables. It would also clarify the issue as to whether the direct integration of the ocean-atmosphere CO_2 flux should be revised to take into account the influence of surfactants.

[49] It is acknowledged that the transfer velocity may be poorly correlated to the wind speed in the presence of surfactants. Other factors, such as the composition and concentration of surfactants, also affects the reduction rate of gas exchange. In addition, both the distribution and movement of surfactants are subjected to greater environmental variations, such as wind-generated surface currents and waves, than is the subsurface water column. These uncertainties provoke recent studies of quantification of atmosphere-ocean gas exchange in terms of parameters more directly related to the transport process, such as short wind waves [e.g., *Bock et al.*, 1999]. Nevertheless, until better parameterization of the gas transfer velocity is established, wind speed will remain the most robust variable in the estimation of global atmosphere-ocean CO_2 flux.

[50] **Acknowledgments.** The authors are grateful to T.-H. Peng and R. Wanninkhof for their help in the calculations of CO_2 fluxes. The constructive comments of W. E. Asher and three anonymous reviewers have led to an improved presentation of these results. Both SSM/I wind speed and AVHRR SST data were obtained from the NASA Physical Oceanography Distributed Active Archive Center at the Jet Propulsion Laboratory of California Institute of Technology. The monthly ΔpCO_2 data of *Takahashi et al.* [1997] were downloaded from the IRI/LDEO Climate Data Library at the Lamont-Doherty Earth Observatory of Columbia University. The data of primary productivity were provided by the Ocean Primary Productivity Research Team at the Institute of Marine and Coastal Sciences of Rutgers University. This work was supported by grants from the National Science Council of Taiwan (NSC 89-2611-M-009-002 and 89-2611-M-009-004).

References

Antoine, D., J.-M. Andre, and A. Morel, Oceanic primary production: 2. Estimation at global scale from Satellite (coastal zone color scanner) chlorophyll, *Global Biogeochem. Cycles*, *10*, 57–69, 1996.

Asher, W. E., The sea-surface microlayer and its effects on global air-sea gas transfer, in *The Sea Surface and Global Change*, edited by P. S. Liss and R. A. Duce, pp. 251–286, Cambridge Univ. Press, New York, 1997.

Asher, W. E., and J. F. Pankow, The interaction of mechanically generated turbulence and interfacial films with a liquid phase controlled gas/liquid transport process, *Tellus, Ser. B*, *38*, 305–318, 1986.

Asher, W. E., L. M. Karle, B. J. Higgins, P. J. Farley, E. C. Monahan, and I. S. Leifer, The influence of bubble plumes on air-seawater gas transfer velocities, *J. Geophys. Res.*, *101*, 12,027–12,041, 1996.

Bates, N. R., and L. Merlivat, The influence of short-term wind variability on air-sea CO_2 exchange, *Geophys. Res. Lett.*, *28*, 3281–3284, 2001.

Behrenfeld, M. J., and P. G. Falkowski, Photosynthetic rates derived from satellite-based chlorophyll concentration, *Limnol. Oceanogr.*, *42*, 1–20, 1997.

Bock, E. J., T. Hara, N. M. Frew, and W. R. McGillis, Relationship between air-sea gas transfer and short wind waves, *J. Geophys. Res.*, *104*, 25,821–25,831, 1999.

Boutin, J., and J. Etcheto, Seasat scatterometer versus Scanning Multichannel Microwave Radiometer wind speeds: A comparison on a global scale, *J. Geophys. Res.*, *95*, 22,275–22,288, 1990.

Boutin, J., and J. Etcheto, Intrinsic error in the air-sea CO_2 exchange coefficient resulting from the use of satellite wind speeds, *Tellus, Ser. B*, *43*, 236–246, 1991.

Boutin, J., J. Etcheto, and P. Ciais, Possible consequences of the chemical enhancement effects for air-sea CO_2 flux estimates, *Phys. Chem. Earth, Ser. B*, *24*, 411–416, 1999.

Broecker, H.-C., and W. Siems, The role of bubbles for gas transfer from water to air at higher wind speed: Experiments in the wind-wave facility in Hamburg, in *Gas Transfer at Water Surface*, edited by W. Brutsaert and G. H. Jirka, pp. 229–236, D. Reidel, Norwell, Mass., 1984.

Broecker, H.-C., J. Petermann, and W. Siems, The influence of wind on CO2-exchange in a wind-wave tunnel, including the effects of monolayers, *J. Mar. Res.*, *36*, 595–610, 1978.

Davies, J. T., The effects of surface films in damping eddies at a free surface of a turbulent liquid, *Proc. R. Soc. London, Ser. A*, *290*, 515–526, 1966.

Esbensen, S. K., and Y. Kushnir, The heat budget of the global ocean: An atlas based on estimates from the surface marine observations, *Clim. Res. Inst. Rep. 29*, Oregon State Univ., Corvalis, 1981.

Etcheto, J., and L. Merlivat, Satellite determination of the carbon dioxide exchange coefficient at the ocean-atmosphere interface: A first step, *J. Geophys. Res.*, *93*, 15,669–15,678, 1988.

Etcheto, J., J. Boutin, and L. Merlivat, Seasonal variation of the CO2 exchange coefficient over the global ocean using satellite wind speeds measurements, *Tellus, Ser. B*, *43*, 247–255, 1991.

Frew, N. M., The role of organic films in air-sea gas exchange, in *The Sea Surface and Global Change*, edited by P. S. Liss and R. A. Duce, pp. 121–172, Cambridge Univ. Press, New York, 1997.

Frew, N. M., J. C. Goldman, M. R. Dennett, and A. S. Johnson, Impact of phytoplankton-generated surfactants on air-sea gas exchange, *J. Geophys. Res.*, *95*, 3337–3352, 1990.

Gašparoviè, B., Z. Kozarac, A. Saliot, B. Ćososović, and D. Möbius, Physicochemical characterization of natural and ex-situ reconstructed sea-surface microlayers, *J. Colloid Interface Sci.*, *208*, 191–202, 1998.

Goldman, J. C., M. R. Dennett, and N. M. Frew, Surfactant effects on air-sea gas exchange under turbulent conditions, *Deep Sea Res.*, *35*, 1953–1970, 1988.

Jähne, B., K. O. Münnich, R. Bosinger, A. Dutzi, W. Huber, and P. Libner, On the parameters influencing air-water gas exchange, *J. Geophys. Res.*, *92*, 1937–1949, 1987a.

Jähne, B., G. Heinz, and W. Dietrich, Measurement of the diffusion coefficients of sparingly soluble gases in water, *J. Geophys. Res.*, *92*, 10,767–10,776, 1987b.

Lefèvre, N., Objective mapping of the seasonal variability ΔpCO_2 in the North Atlantic ocean, *Global Atmos. Ocean Syst.*, *5*, 247–271, 1997.

Lefèvre, N., A. J. Watson, D. J. Cooper, R. F. Weiss, T. Takahashi, and S. C. Sutherland, Assessing the seasonality of the oceanic sink for CO_2 in the Northern Hemisphere, *Global Biogeochem. Cycles*, *13*, 273–286, 1999.

Lin, I. I., L. S. Wen, K.-K. Liu, W. Tsai, and A. K. Liu, Evidence and quantification of the correlation between radar backscatter and ocean color supported by simultaneously acquired in situ sea truth, *Geophys. Res. Lett.*, *29*(10), 1464, doi:10.1029/2001GL014039, 2002.

Liss, P. S., and L. Merlivat, Air-sea gas exchange rates: Introduction and synthesis, in *The Role of Air-Sea Exchange in Geochemical Cycling*, edited by P. Buat-Menard, pp. 113–127, D. Reidel, Norwell, Mass., 1986.

Liu, A. K., S. Y. Wu, W. Y. Tseng, and W. G. Pichel, Wavelet analysis of SAR images for coastal monitoring, *Can. J. Remote Sens.*, *26*, 494–500, 2000.

Longhurst, A. R., S. Sathyendranath, T. Platt, and C. Caverhill, An estimation of global primary production in the ocean from satellite radiometer data, *J. Plankton Res.*, *17*, 1245–1271, 1995.

Merlivat, L., and L. Memery, Gas exchange across an air-water interface. Experimental results and modeling of bubble contribution to transfer, *J. Geophys. Res.*, *88*, 707–724, 1983.

Robertson, J. E., and A. J. Watson, Thermal skin effect of the surface ocean and its implications for CO_2 uptake, *Nature*, *358*, 738–740, 1992.

Takahashi, T., T. T. Takahashi, and S. C. Sutherland, An assessment of the role of the North Atlantic as a CO_2 sink, *Phil. Trans. R. Soc. London, Ser. B*, *348*, 143–152, 1995.

Takahashi, T., R. A. Feely, R. F. Weiss, R. H. Wanninkhof, D. W. Chipman, S. C. Sutherland, and T. T. Takahashi, Global air-sea flux of CO_2: An estimate based on measurement of sea-air pCO_2 difference, *Proc. Natl. Acad. Sci. USA*, *94*, 8292–8299, 1997.

Takahashi, T., R. H. Wanninkhof, R. A. Feely, R. F. Weiss, D. W. Chipman, N. Bates, J. Olafsson, C. Sabine, and S. C. Sutherland, Net sea-air CO_2 flux over the global oceans: An improved estimate based on the sea-air pCO_2 difference, in *Proceedings of Second International Symposium on CO_2 in the Oceans*, edited by Y. Nojiri, pp. 9–18, Cent. for Global Environ. Res., NIEST, Tsukuba, Japan, 1999.

Tsai, W.-T., Impact of a surfactant on a turbulent shear layer under the air-sea interface, *J. Geophys. Res.*, *101*, 28,557–28,568, 1996.

Tsai, W.-T., Vortex dynamics beneath a surfactant contaminated ocean surface, *J. Geophys. Res.*, *103*, 27,919–27,930, 1998.

Van Scoy, K. A., K. P. Morris, J. E. Robertson, and A. J. Watson, Thermal skin effect and the air-sea flux of carbon dioxide: A seasonal high-resolution estimate, *Global Biogeochem. Cycles*, *9*, 253–262, 1995.

Vazquez, J., A. V. Tran, R. Sumagaysay, and E. Smith, *NOAA/NASA AVHRR Oceans Pathfinder Sea Surface Temperature User Reference Manual*, Jet Propul. Lab., Pasadena, Calif., 1996.

Wanninkhof, R., Relationship between wind speed and gas exchange over the ocean, *J. Geophys. Res.*, *97*, 7373–7382, 1992.

Wanninkhof, R., J. R. Ledwell, and W. S. Broecker, Gas exchange-wind speed relation measured with sulfur hexafluoride on a lake, *Science*, *227*, 1224–1226, 1985.

Weiss, R. F., Carbon dioxide in water and seawater: The solubility of a nonideal gas, *Mar. Chem.*, *8*, 203–215, 1974.

Wentz, F. J., A well-calibrated ocean algorithm for Special Sensor Microwave/Imager, *J. Geophys. Res.*, *102*, 8703–8718, 1997.

Wilson, W. B., and A. Collier, The production of surface-active material by marine phytoplankton cultures, *J. Mar. Res.*, *30*, 15–26, 1972.

Žutić, V., B. Ćosović, E. Marèenko, and N. Bihari, Surfactant production by marine phytoplankton, *Mar. Chem.*, *10*, 505–520, 1981.

W.-T. Tsai, Institute of Hydrological Sciences, National Central University, Jungli City, Taoyuan 320, Taiwan. (wttsai@cc.ncu.edu.tw)

K.-K. Liu, Institute of Oceanography, National Taiwan University and National Center for Ocean Research, Taipei 106, Taiwan. (kkliu@ccms.ntu.edu.tw)